Open Access Articles

Citation	
DOI	
Publisher	
Version	
Terms of Use	

Oregon State UNIVERSITY OSU

Superior Cathode of Sodium-Ion Batteries: Orthorhombic V_2O_5 Nanoparticles Generated in Nanoporous Carbon by Ambient Hydrolysis Deposition

Vadivukarasi Raju,† Jordan Rains,† Cooper Gates,† Wei Luo,† Xingfeng Wang,† William F. Stickle,‡ Galen D. Stucky§ and Xiulei Ji†*

†Department of Chemistry, Oregon State University, Corvallis, Oregon, 97331-4003, USA

§Department of Chemistry and Biochemistry, University of California, Santa Barbara, California, 93117-9510, USA

‡Hewlett-Packard Co., 1000 NE Circle Blvd., Corvallis, Oregon, 97330, USA

ABSTRACT. We, for the first time, demonstrate that orthorhombic V_2O_5 can exhibit superior electrochemical performance in sodium ion batteries when uniformly coated inside nanoporous carbon. The encapsulated V_2O_5 shows a specific capacity as high as 276 mAh/g, while the whole nanocomposite exhibits a capacity of 170 mAh/g. The V_2O_5/C composite was fabricated by a novel ambient hydrolysis deposition that features sequential water vapor adsorption in nanoporous carbon, followed by a hydrolysis reaction, exclusively inside the nanopores. The unique structure of the nanocomposite significantly enhances the capacity as well as the rate performance of orthorhombic V_2O_5 where the composite retains a capacity of over 90 mAh/g at a current rate of 640 mA/g. Furthermore, by calculating, we also revealed that a large portion of the sodium-ion storage, particularly at high current rates, is due to the V_2O_5 pseudocapacitance.

Currently, portable electronics and electric vehicles are highly dependent on lithium-ion batteries (LIBs). However, concerns on Li rarity and its uneven geographical distribution have prompted researchers to search for alternative solutions for energy storage.[1] Sodium-ion batteries (SIBs) represent one of the most promising options due to its low cost, abundance and distribution all over the world.[2] As an emerging technology, SIBs is limited by a lack of high-performance electrodes.[3]

Not surprisingly, many cathode candidates for SIBs are borrowed from LIBs,[4,5,6,7] such as layered transition metal oxides,[8,9,10] metal phosphates,[11,12] and Prussian blue analogs.[13,14] Among them, V_2O_5, as a promising material, has exhibited great performance in LIBs.[15,16,17,18,19,20,21] Early studies showed that V_2O_5 aerogels can perform reversible sodium insertion/deinsertion.[22] Recently, Tepavcevic et al. and Su et al. reported that bilayered V_2O_5 materials exhibit a high capacity, above 170 mAh/g, as well as stable cycling performance in SIBs[23,24] Compared to the bilayered V_2O_5, bulk orthorhombic V_2O_5 exhibits a much lower capacity, 60 mAh/g.[24] For orthorhombic V_2O_5, the major hurdle is the slow sodium-ion diffusion in the compact crystal structure.[25] To tackle this challenge, one approach adopted in LIBs is to decrease dimensions of V_2O_5 and coat it on conductive substrates.[26,27,28 29]

Herein, we report that orthorhombic V_2O_5 nanoparticles, 5-7 nm in size, encapsulated in nanoporous carbon exhibit excellent electrochemical performance in SIBs. Recently, our group has invented an ambient hydrolysis deposition (AHD) methodology that features sequential water vapor adsorption in nanoporous carbon, followed by a hydrolysis reaction, exclusively inside nanopores, in non-aqueous solution. It is very effective to generate conformal coating of metal oxides on the surface of porous carbons. [30,31] The AHD method allows us, for the first

time, to control the loading levels of V_2O_5 in nanoporous carbon and reveal the electrochemical properties of orthorhombic V_2O_5 nanoparticles as a cathode in SIBs.

We prepared the nanoporous carbon according to the well-established procedure by using resorcinol (1,3-dihydroxybenzene) and formaldehyde (HCHO) as precursors.[32] The nanoporous carbon is referred to as RFC. V_2O_5/C composites were prepared via the AHD method. Briefly, nanoporous carbon was exposed to water vapor at 80 °C for one hour. Then, the nanoporous carbon with water preloaded was dispersed in a cyclohexane solution of vanadium triisopropoxide (10 vol%). After soaking for one hour, the solid product was collected by filtration in glovebox before heating in air at 225 °C to eliminate the organic moieties. We repeated the above AHD cycle for various times to achieve the desired loading levels of V_2O_5 in the nanocomposites. The obtained composites are denoted as X-V_2O_5-RFC, where X represents the weight percentage of V_2O_5 in the composites.

We measured the V_2O_5 loading in the nanocomposites by thermogravimetric analysis (TGA) in air. **Figure 1a** shows the TGA data for V_2O_5-RFC composites obtained after various AHD cycles. For pure RFC, weight loss due to carbon oxidation occurs from at 500 °C (Supporting Information **Figure S1**). For the V_2O_5-RFC samples, the oxidation onset temperature dramatically drops from 500 °C to 300 °C, which implies that the coated vanadium oxide catalyses carbon oxidation. With one AHD cycle, the TGA plot displays two well-defined weight losses, from 300 °C to 375 °C and from 400 °C to 500 °C, respectively. The lower-temperature weight loss should be attributed to the carbon oxidation catalysed by vanadium oxide while the higher temperature weight loss corresponds to the non-catalysed oxidation of carbon in air. Two-carbon-oxidation events indicate that, the first AHD cycle does not construct a continuous V_2O_5 coating on RFC. Interestingly, after the second AHD cycle, with 37wt% of V_2O_5 loaded in the

4

composite, only one slopping weight loss region is observed. After the third and the fifth AHD cycle, the weight loss at higher temperature regions further diminished, which indicates repeated AHD cycles improve V_2O_5 coverage on carbon surface.

We characterized the structure of V_2O_5 in the nanocomposites by XRD, as **Figure 1b** shows. We also looked at bulk vanadium oxide formed by hydrolysis of the same precursor in a petri dish (Supporting Information **Figure S2**). As expected, all nanocomposites exhibit much broadened peaks due to the small particle sizes, which can still be assigned to the orthorhombic phase of V_2O_5. The major XRD peak from the V_2O_5/C nanocomposite at ~26° matches the peak (110) displayed by the bulk V_2O_5 formed by the same hydrolysis method. By comparing this XRD pattern from the nanocomposite to the XRD patterns of bi-layered V_2O_5 in literature, it is clear that the nanoparticles in the composites are not of a bi-layered structure.[23,24] These nanoparticles formed by the AHD coating are most likely orthorhombic. With more AHD cycles, the domain size of the deposited V_2O_5 is larger. Estimated by the Scherrer Equation, the domain size increases from 5 to 7 nm from 55-V_2O_5-RFC (after three AHD cycles) to 70-V_2O_5-RFC (after five AHD cycles).

Surface area and porosity characteristics of the composites were analysed by N_2 sorption measurements, and the results are summarized in Supporting Information **Table S1**. RFC exhibits a specific surface area and pore volume of 1081 m^2/g and 5.3 cm^3/g, respectively, and an average pore size of 39 nm. After impregnating 55 wt% of V_2O_5, the specific surface area and pore volume of the composite drops to 641 m^2/g and 2.9 cm^3/g, respectively. With 70 wt% V_2O_5 loaded, these parameters further decrease to 463 m^2/g and 2.6 cm^3/g, indicating an effective pore filling inside RFC framework. By loading 55 wt% and 70 wt% of V_2O_5 in the RF carbon, 6.8% and 13.1% of the available pore volume was filled by V_2O_5 in the composite.

We further identified the chemical compositions of the vanadium oxide coated on carbon by X-ray photoelectron spectroscopy (XPS) where the V $2p_{2/3}$ peak can be deconvoluted into two binding energies: 515.5 eV and 517.3 eV, corresponding to V^{5+} and V^{4+}, respectively (**Figure 1c and d**). The V^{4+}/V^{5+} ratio is ~16%, for both 55-V_2O_5-RFC and 70-V_2O_5-RFC. The results suggest the presence of oxygen vacancies in the V_2O_5 lattice. Previous studies on V_2O_5 for LIBs implied that such vacancies may enhance the electrochemical performance of V_2O_5 samples.[33]

An important task is to reveal whether or not V_2O_5 has been completely encapsulated into the pores of nanoporous carbon. To address this question, we first compared the surface morphology of RFC and 55-V_2O_5-RFC by scanning electron microscopy (SEM), where we could not identify any difference (**Figure 2a, b** and **c**). However, with a higher loading of 70 wt% V_2O_5, needle-like particles of V_2O_5 appear on the surface of carbon (**Figure 2d**). Certainly, there is a limit for the exclusive interior coating even though the specific pore volume of RFC allows 94 wt% V_2O_5 to be loaded. We then studied how V_2O_5 is distributed in 55-V_2O_5-RFC by transmission electron microscopy (TEM). As **Figure 3a** shows, 55-V_2O_5-RFC exhibits a highly porous structure. Furthermore, it is evident that the AHD-deposited vanadium oxide is, indeed, uniformly dispersed in the porous carbon framework, judged based on the high-angle angular dark field scanning TEM (HAADF-STEM) and the corresponding energy-dispersive X-ray spectroscopy (EDX) elemental mapping (**Figure 3b-d**).

The primary goal of the study is to find out whether or not nanoparticles of orthorhombic V_2O_5 exhibit any enhanced electrochemical performance in SIBs. We assembled coin cells with the composites as the working electrode and sodium foil as the counter/reference electrode. Initial electrochemical analyses were conducted at a current density of 40 mA/g in a potential window from 1.5 to 3.8 V vs. Na^+/Na. **Figure 4a** shows the charge-discharge profiles for RFC, 37-V_2O_5-

RFC, 55-V_2O_5-RFC, and 70-V_2O_5-RFC composites. Nearly linear voltage profiles were observed as a function of inserted sodium ions in V_2O_5-RFC composites. Composites of 37-V_2O_5-RFC and 55-V_2O_5-RFC exhibit a discharge capacity of 123 mAh/g and 183 mAh/g, respectively, while RFC also shows a capacity of 48 mAh/g due to the electrical double layer capacitance. Note that the specific capacity is calculated based on the total mass of the composites. **Figure 4 b** shows the initial cycling performance of RFC, 55-V_2O_5-RFC and 70-V_2O_5-RFC. If we assume RFC in the composites contributes the same capacity as in its pure form to the capacity of the composites, we can estimate the specific capacity of V_2O_5 in the 55-V_2O_5-RFC to be 276 mAh/g. This is one of the highest capacity values reported for orthorhombic V_2O_5 in SIBs. Since the cutoff potential of 1.5 V was chosen arbitrarily, it is, in fact, very difficult to predict the exact oxidation state of vanadium at this potential. If we consider this is a two-electron transfer and assume that all the vanadium is in the oxidation state 5+, the theoretical capacity is 294 mAh/g. In our case, ~16 % of vanadium is in the oxidation state 4+, as revealed by the XPS results, and the theoretical capacity for vanadium oxide in our nanocomposite should be 247 mAh/g. This is significantly lower than our experimental observation. Therefore, at 1.5 V versus Na^+/Na, we hypothesize that the oxidation state of vanadium is in fact a mixture of 4+ and 3+.

The charge/discharge profile for the third cycle of 55-V_2O_5-RFC is shown in Supporting Information **Figure S3**. The 55-V_2O_5-RFC composite exhibits a columbic efficiency of 93-95%. Surprisingly, 70-V_2O_5-RFC with more V_2O_5 loading exhibits a similar capacity as 55-V_2O_5-RFC does. This implies that the sodium-ion storage in V_2O_5 may partially originate from a surface pseudocapacitance and more V_2O_5 loading does not necessarily increase the surface area of active mass. For comparison, we also analysed bulk V_2O_5 electrode under the same conditions,

which exhibits a much lower specific capacity of 15 mAh/g (**Figure 4a**). The poor performance of the bulk orthorhombic V_2O_5 is consistent with the earlier reports.[24]

We chose to focus on 55-V_2O_5-RFC to further understand the electrochemical performance of the AHD-enabled composites. Cyclic voltammetry (CV) scans were carried out at a sweeping rate of 0.5 mV/s in the voltage window from 1.5 to 3.8 V vs. Na^+/Na. As **Figure 4c** shows, during the first cathodic scan, a broad reduction peak occurs from 3 to 2.25 V, followed by another one from 2.0 to 1.5 V. As revealed by XPS (**Figure 1c,d**), vanadium in the composites is mainly in the oxidation state of V^{5+}. Thus, the two sequential cathodic peaks may be ascribed to the reduction processes from V^{5+} to V^{4+} and from V^{4+} to V^{3+}, respectively. In the first anodic scan, the broad 'hill' should be ascribed to the desodiation process. Interestingly, in the second and third anodic scans, the oxidation current evolves into two better resolved peaks: one centered at ~2.3 V and the other at ~3.0 V, which may suggest the sequential extraction of sodium ions from V_2O_5. We also found out that 55-V_2O_5-RFC exhibits better kinetics than 70-V_2O_5-RFC, which is evident by comparing the redox peak separation in CV curves (Supporting Information **Figure S4**). This should be correlated with the smaller particle size of V_2O_5 in 55-V_2O_5-RFC.

We characterized the rate performance of 55-V_2O_5-RFC at different galvanostatic current densities, as shown in **Figure 4d**. Impressively, the composite retains 52 % of its capacity when the rate was increased by 16 times from 40 to 640 mA/g. This is comparable to the high rate performance from the bilayered materials.[24] Interestingly, there is a plateau centred on 2.7 V during the charging process, which becomes more pronounced at higher current rates. This indicates that the desodiation may occur through different pathways compared to the sodiation process. Ongoing research is untaken to further investigate this interesting phenomenon. **Figure**

4e shows the cycling performance of 55-V$_2$O$_5$-RFC over 70 cycles at different current densities, where after 70 cycles, a specific capacity of 140 mAh/g was retained at 40 mA/g.

Due to the small particle sizes of V$_2$O$_5$, we expect that the composite may exhibit significant pseudocapacitance.[34] In fact, V$_2$O$_5$ nanosheets,[35] V$_2$O$_5$/carbon nanotubes[36] and porous V$_2$O$_5$/C composites[37] have been studied for pseudocapacitor applications. It is necessary to deconvolute total current based on two different charge-storage mechanisms: the diffusion-controlled Faradaic reaction and the capacitive behaviour, including the surface pseudocapacitance and the non-Faradaic electrical double layer capacitance.[38] Accordingly, the current response (*i*) at a fixed potential (*V*) can be represented by the following equation:

$$i\ (V) = k_1 v + k_2 v^{1/2}$$

where, $k_1 v$ represents the total capacitive contribution while $k_2 v^{1/2}$ stands for the contribution of diffusion-controlled Faradaic intercalation process. The linear plot of $i/v^{1/2}$ as a function of $v^{1/2}$ was used to determine the slope (k_1) and intercept (k_2) (Supporting Information **Figure S5**). By determining the value of k_1 and k_2, we are able to estimate capacitive charge storage at a certain voltage.

Our results show that the capacitive charge storage is a significant contributor to the total capacity, particularly at high sweeping rates. CV curves of 55-V$_2$O$_5$-RFC at sweeping rates from 0.5 mV/s to 20 mV/s between 1.5 V to 3.8 V vs. Na$^+$/Na were used to quantify the capacitive contribution (**Figure 5 a**). **Figure 5 b** and Supporting Information **Figure S6** show the CV profiles for the calculated capacitive current and the total measured current for 55-V$_2$O$_5$-RFC at a sweep rate of 5 mV/s and 0.5 mV/s, respectively. At 0.5 mV/s, the capacitive process accounts for only ~20 % of the total charge storage, estimated by the enclosed area, while at 5 mV/s, this

value increases to about 40%. Furthermore, it is evident that the current from diffusion-controlled redox reactions dominate from 2.5 to 3 V. At the potentials lower or higher, the current response comprises a significant capacitive portion.

In order to further differentiate pseudocapacitive behaviour from the double layer capacitance, we employed an electrolyte with very large ions that cannot be inserted into V_2O_5, namely, 1.0 M tetraethylammonium (TEA^+) tetrafluoroborate (BF_4^-) in propylene carbonate. The obtained capacitance is less than 5% of the total charge storage. This means that the majority of the capacitive charge storage is due to the pseudocapacitance of V_2O_5 (Supporting Information **Figure S7**). The high pseudocapacitance is due to the high surface area of coated V_2O_5 in porous carbon, as evident by the vast difference between CV profiles of 55-V_2O_5-RFC and bulk V_2O_5 (**Figure 5 c**).

In order to further understand the electrochemical properties of the materials, electrochemical impedance spectroscopy (EIS) measurements were carried out on bulk V_2O_5, RFC and 55-V_2O_5-RFC at a frequency range of 200 KHz to 10 mHz with a signal amplitude of 10 mV. As **Figure 5 d** shows, all the Nyquist plots feature two well-defined regions, a depressed semi-circle followed by an inclined straight line at the low frequency region. **Figure 5e inset** shows the equivalent circuit that gives rise to a good fit for the EIS spectra of 55-V_2O_5-RFC and bulk V_2O_5 (see **Figure S8**) with the fitting parameters presented in **Table S2**. In the equivalent circuit, R_s represents the equivalent series resistance (ESR) that includes all Ohmic resistance due to the electrolyte and other parts of the cell. C_{dl} and C_f are the constant phase elements (CPE), revealing the non-ideal capacitance due to the surface roughness, while R_{ct} and R_f stand for the charge transfer resistance through the electrode/electrolyte interface and the contacts in between V_2O_5 particles, respectively. The Warburg element, W, reflects the solid-state diffusion of Na^+

ions inside the V_2O_5 particles.[39,40] It is worth noting that 55-V_2O_5-RFC exhibits a much smaller R_f (1.5 Ω) than that of bulk V_2O_5 (24.7 Ω), which should be attributed to the smaller particle sizes of V_2O_5.

In conclusion, we, for the first time, observed superior electrochemical performance of orthorhombic V_2O_5 that is encapsulated in nanoporous carbon. In the V_2O_5/C nanocomposites, the loading levels of V_2O_5 can be controlled by adjusting the number of AHD cycles. As a promising cathode material for SIBs, V_2O_5-RFC composites exhibit a reversible capacity of over 170 mAh/g at 40 mA/g and 92 mAh/g at a very high current density of 640 mA/g. In 55-V_2O_5-RFC, V_2O_5 alone exhibits an impressive specific capacity of 276 mAh/g. By modelling, we revealed the pseudocapacitance behaviour of orthorhombic V_2O_5 nanoparticles that accounts for a significant portion of the total capacity. The excellent electrochemical properties of V_2O_5-RFC composites can be attributed to the small particle sizes, fine dispersion and controlled loading of V_2O_5 in nanoporous carbon.
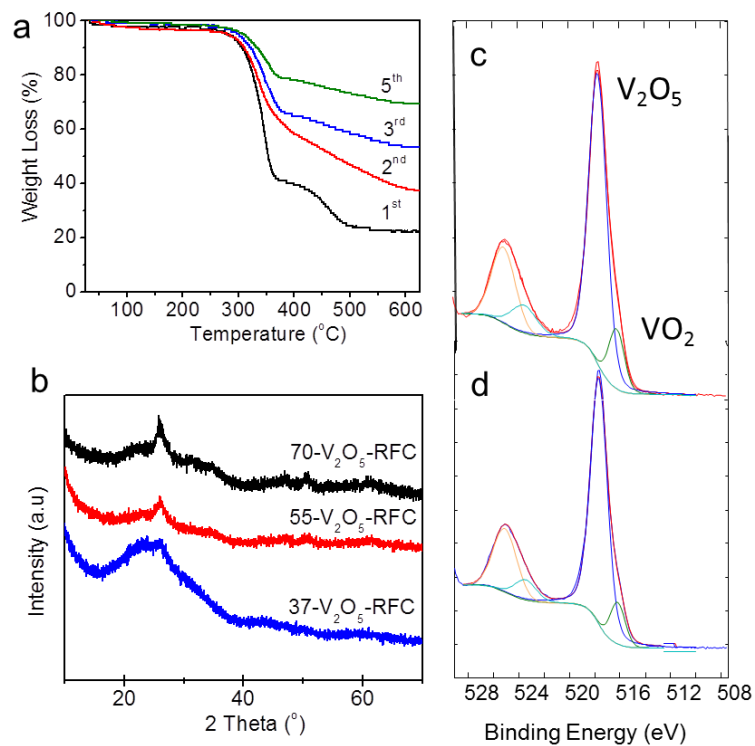
Figure 1. (a) TGA profiles of V_2O_5-RFC nanocomposites after 1st to 5th AHD loading. (b) XRD patterns of 37-V_2O_5-RFC, 50-V_2O_5-RFC, and 70-V_2O_5-RFC. (c, d) XPS spectra of 55-V_2O_5-RFC and 70-V_2O_5-RFC, respectively.
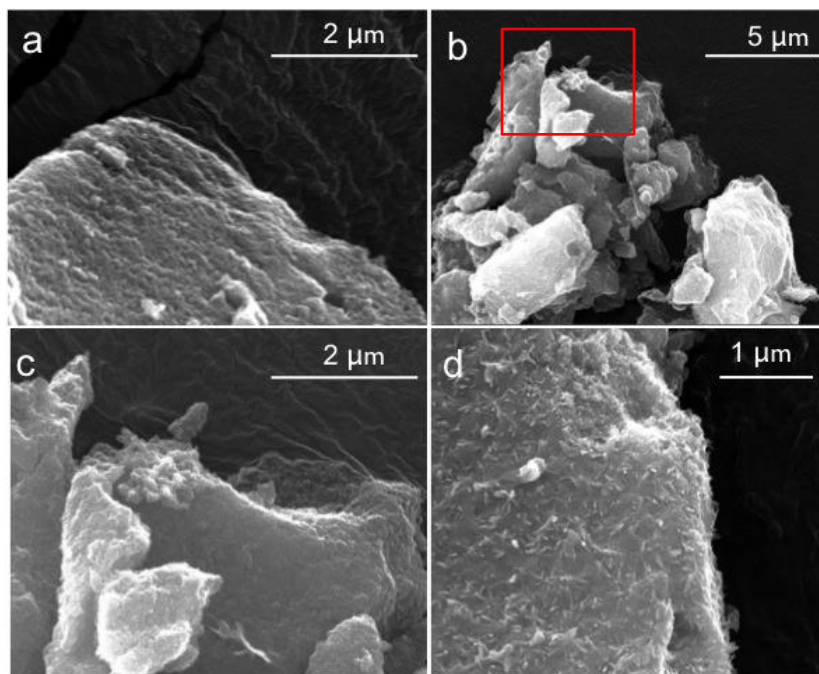
Figure 2. (a) SEM image of RFC. (b) SEM images of 55-V_2O_5-RFC. (c) Expansion of the area marked by the red-box in b. (d) SEM image of 70-V_2O_5-RFC.
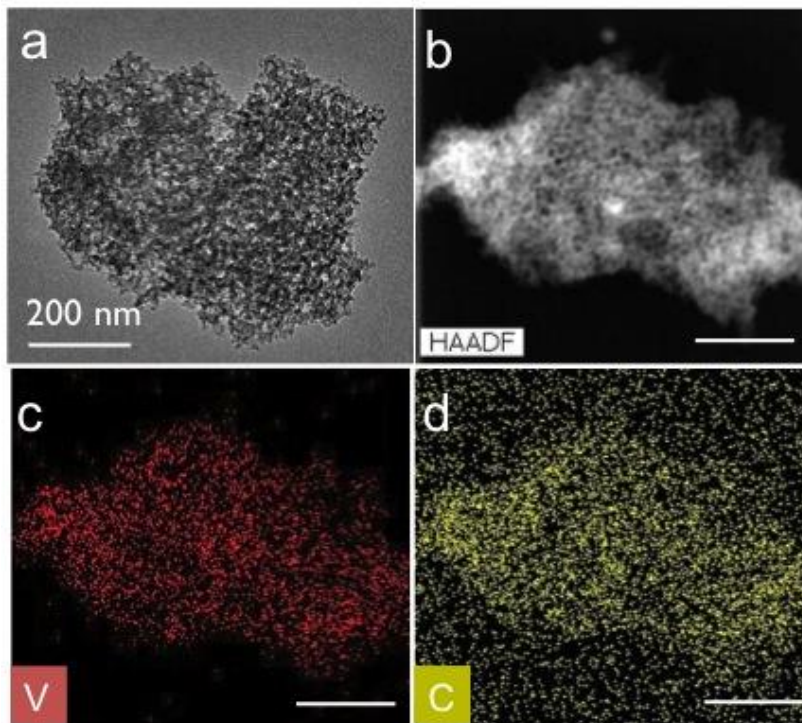
Figure 3. (a) TEM image of 55-V$_2$O$_5$-RFC. (b) HAADF-STEM image of 55-V$_2$O$_5$-RFC and the corresponding EDX mappings of (c) vanadium and (d) carbon, respectively (scale bar = 200 nm).
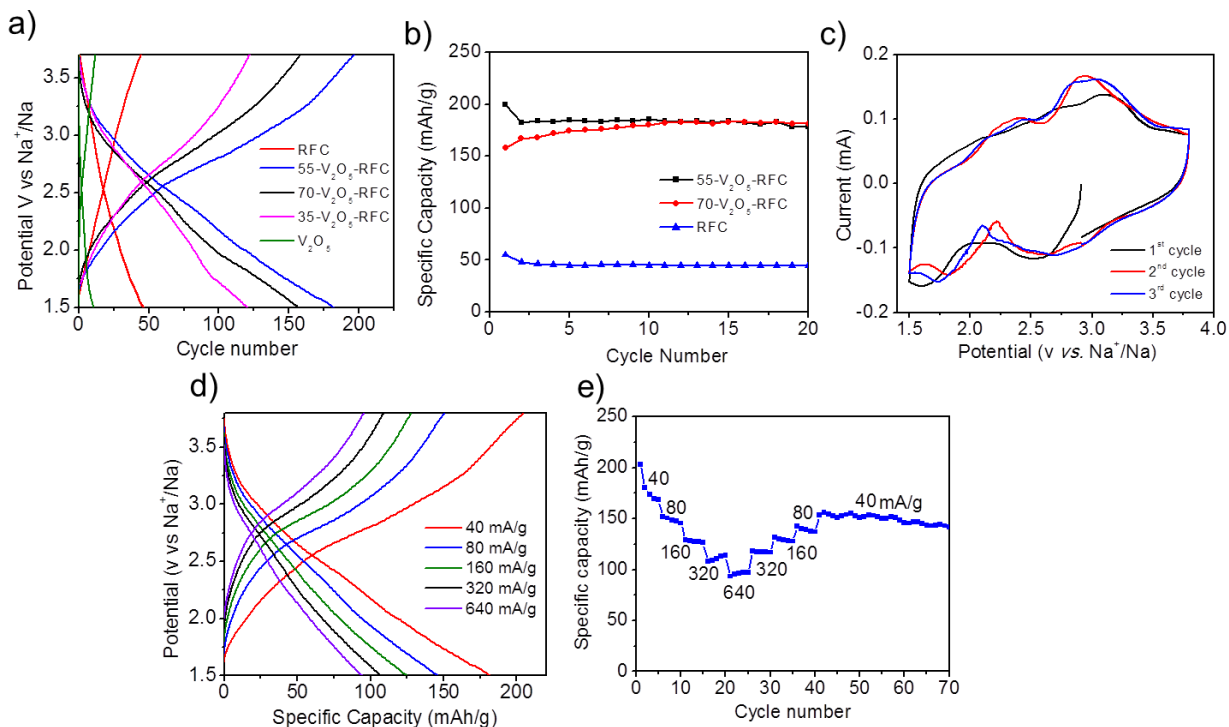
Figure 4. (a) Galvanostatic charge-discharge profiles of RFC, 37-V_2O_5-RFC, 55-V_2O_5-RFC, 70-V_2O_5-RFC and bulk V_2O_5 at 40 mA/g between 1.5 V to 3.8 V in 1.0 M $NaClO_4$/PC. (b) Initial cycling performance of RFC, 55-V_2O_5-RFC and 70-V_2O_5-RFC. (c) CV profiles for the first three cycles of 55-V_2O_5-RFC at a scanning rate 0.5 mV/s. (d) Galvanostatic charge-discharge profiles of 55-V_2O_5-RFC at current densities of 40, 80, 160, 320 and 640 mA/g (e) Rate and cycling performance of 55-V_2O_5-RFC.
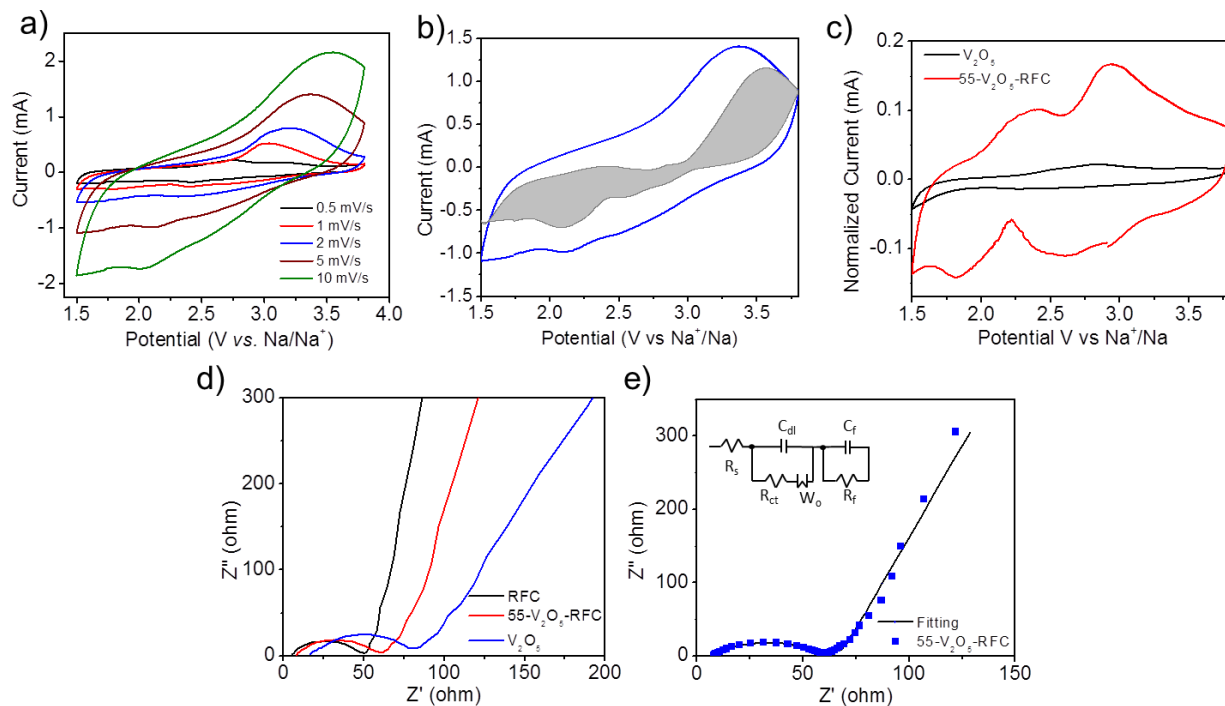
Figure 5. (a) CV profiles of 55-V$_2$O$_5$-RFC at different scanning rates from 0.5 mV/s to 10 mV/s. (b) CV profile for 55-V$_2$O$_5$-RFC at a sweeping rate of 5 mV/s. The estimated capacitive current contribution is shown in the shaded region. (c) CV profiles of bulk V$_2$O$_5$ and 55-V$_2$O$_5$-RFC at 0.5 mV/s. (d) Nyquist plots of RFC, 55-V$_2$O$_5$-RFC and bulk V$_2$O$_5$. (e) Fitting for the Nyquist plot of 55-V$_2$O$_5$-RFC, Inset: equivalent circuit.

TOC
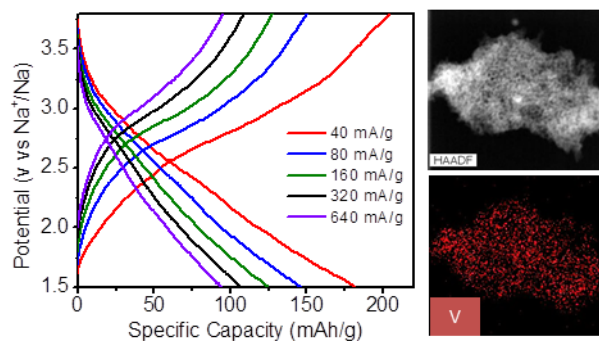
ASSOCIATED CONTENT

Supporting Information. Experimental section, characterization details, and supporting data.

This material is available free of charge via the Internet at http://pubs.acs.org.

AUTHOR INFORMATION

Corresponding Author

*E-Mail: David.Ji@oregonstate.edu

Notes

The authors declare no competing financial interest.

REFERENCES

[1]   Tarascon, J. M. *Nat. Chem.* **2010,** 2, 510-510.

[2]   Palomares, V.; Cabanas, M.C-.; Martinez, E. C.; Han, M. H.; Rojo, T. *Energy Environ. Sci.* **2013,** 6, 2312-2337.

[3]   Pan, H.; Hu, Y. S.; Chen, L. *Energy Environ. Sci.* **2013,** 6, 2338-2360.

[4]   Ellis, B. L.; Nazar, L. F. *Curr. Opin. Solid State Mater. Sci.* **2012,** 16, 168-177.

[5]   Slater, M. D.; Kim, D.; Lee, E.; Johnson, C. S. *Adv. Funct. Mater.* **2013,** 23, 947-958.

[6]   Ha, K. H.; Woo, S. H.; Mok, D.; Choi, N. S.; Park, Y.; Oh, S. M.; Kim, Y.; Kim, J.; Lee, J.; Nazar, L. F.; Lee , K. T. *Adv. Energy Mater.* **2013,** 3, 770-776.

[7]   Langrock, A; Xu, Y.; Liu, Y.; Ehrman, S.; Manivannan, A.; Wang, C. *J. Power Sources* **2012,** 223, 62-67.

[8]   Berthelot, R.; Carlier, D.; Delmas, C. *Nat. Mater.* **2011,** 10, 74-80.

[9]   Xia, X.; Dahn, J. R. *Electrochem. Solid-State Lett.* **2012,** 15, A1-A4.

[10] Su, D.; Wang, C.;Ahn, H. J.; Wang, G. *Chem. Eur. J* **2013,** 19, 10884-10889.

[11] Liu, Y.; Xu, Y.; Han, X.; Pellegrinelli, C.; Zhu, Y.; Zhu, H.; Wan, J.A.; Chung, C.; Vaaland, O.; Wang, C.; Hu, L. *Nano Lett.* **2012,** 12, 5664-5668.

[12] Lee, K. T.; Ramesh, T. N.; Nan, F.; Botton, G.; Nazar, L. F. *Chem. Mater.* **2011,** 23, 3593-3600.

[13] Lu, Y.; Wang, L.; Cheng, J.; Goodenough, J. B. *Chem. Commun.* **2012,** 48, 6544- 6546.

[14] Jian, Z.; Han, W.; Lu, X.; Yang, H.; Hu, Y-S.; Zhou, J.; Zhou, Z.; Li, J.; Chen, W.; Chen, D.; Chen, L. *Adv. Energy Mat.* **2013,** 3, 156-160.

[15] Zhang, C.; Chen, Z.; Guo, Z.; Lou, X. W. *Energy Environ. Sci.* **2013,** 6, 974-978.

[16] Wu, H. B.; Pan, A.; Hng, H. H.; Lou, X. W. *Adv. Funct. Mater.* **2013,** 23, 5669-5674.

[17] Whittingham, M. S. *Chem. Rev.* **2004,** 104, 4271-4301.

[18] Mai, L; Xu, L.; Han, C.; Xu. X.; Luo, Y.; Zhao, S.; Zhao, Y. *Nano Lett.* **2010,** 10, 4750-4755.

[19] Mai, L.; Dong, F.; Xu, X.; Luo, Y.; An, Q.; Zhao, Y.; Pan, J.; Yang, J. *Nano Lett.* **2013,** 13, 740-745.

[20] Mai, L.; An, Q.; Wei, Q.; Fei, J.; Zhang, P.; Xu, X.; Zhao, Y.; Yan, M.; Wen, W.; Xu, L. *Small* **2014,** DOI: 10.1002/smll.201302991.

[21] An, Q.; Zhang, P.; Wei, Q.; He, L.; Xiong, F.; Sheng, J.; Wang, Q.; Mai, L. *J. Mater. Chem. A.* **2014,** 2, 3297-3302.

[22] Tang, P. E.; Sakamoto, J.; Baudrin, S.E.; Dunn, B. *J. Non-Cryst. Solids*. **2004,** 350, 67-72

[23] Tepavcevic, S.; Xiong, H.; Stamenkovic, V. R.; Zuo, X.; Balasubramanian, M.; Prakapenka, V. B.; Johnson, C. S.; Rajh, T. *ACS Nano* **2012,** 6, 530-538.

[24] Su, D.; Wang, G. *ACS Nano,* **2013,** 7, 11218-11226.

[25]   Badot, J. C.; Baffier, N. *J. mater. Chem.* **1992,** 2, 1167-1175.

[26]   Chen, X.; Zhu, H.; Chen, Y. C.; Shang, Y.; Cao, A.; Hu, L.; Rubloff, G. W. *ACS Nano.* **2012,** 6, 7948-7955.

[27]   Yan, J.; Sumboja, A.; Khoo, E.; Lee, P. S. *Adv. Mater.* **2011,** 23, 746-750.

[28]   Liu, J.; Xia, H.; Xue, D.; Lu, L. *J. Am. Chem. Soc.* **2009,** 131, 12086-12087.

[29]   Yu, X.; Pan, H.; Wan, W.; Ma, C.; Bai, J.; Meng, Q.; Ehrlich, S. N.; Hu, Y-S.; Yang, X-Q. *Nano Lett.* **2013,** 13, 4721-4727.

[30]   Wang, X.; Raju, V.; Luo, W.; Wang, B.; Stickle, W. F.; Ji, X. *J. Mater. Chem. A* **2014,** 2, 2901-2905.

[31]   Raju, V.; Wang, X.; Luo, W.; Ji, X. *Chem. Eur. J* **2014,** 20, 1-7.

[32]   Han, S.; Hyeon, T. *Chem. Commun.* **1999,** 1955-1956.

[33]   Liu, D.; Liu, Y.; Pan, A.; Nagle, K. P.; Seidler, G. T.; Jeong, Y. H.; Cao, G. *J. Phys. Chem. C* **2011,** 115, 4959-4965.

[34]   Yu, G.; Hu, L.; Vosgueritchian, M.; Wang, H.; Xie, X.; McDonough, J. R.; Cui, X.; Cui, Y.; Bao, Z. *Nano Lett.* **2011,** 11, 2905-2911.

[35]   Zhu, J.; Cao, L.; Wu, Y.; Gong, Y.; Liu, Z.; Hoster, H. E.; Zhang, Y.; Zhang, S.; Yang, S.; Yan, Q.; Ajayan, P. M.; Vajtai, R. *Nano Lett.* **2013,** 13, 5408-5413.

[36]   Boukhalfa, S.; Evanoff, K.; Yushin, G. *Energy Environ. Sci.* **2012,** 5, 6872-6879.

[37] Chen, Z.; Augustyn, V.; Jia, X.; Xiao, Q.; Dunn, B.; Lu, Y. *ACS Nano* **2012,** 6, 4319-4327.

[38] Wang, J.; Polleux, J.; Lim, J.; Dunn, B. *J. Phys. Chem. C* **2007,** 111, 14925-14931.

[39] Zhu, Y.; Xu, Y.; Liu, Y.; Luo, C.; Wang, C. *Nanoscale,* **2013,** 5, 780-787.

[40] Ruffo, R.; Hong, S. S.; Chan, C. K.; Huggins, R. A.; Cui, Y. *J. Phys. Chem. C* **2009,** 113, 11390-11398.